SPIRAL GROOVE FACE SEAL CONCEPTS; COMPARISON TO CONVENTIONAL FACE CONTACT SEALS IN SEALING LIQUID SODIUM (400° to 1000° F)

by Thomas N. Strom, Lawrence P. Ludwig, Gordon P. Allen,

and Robert L. Johnson

Lewis Research Center
Cleveland, Ohio

TECHNICAL PAPER proposed for presentation at

Seal Symposium
sponsored by the American Society of Mechanical Engineers
Pittsburgh, Pennsylvania, November 12-16, 1967

NATIONAL AERONAUTICS AND SPACE ADMINISTRATION

SPIRAL GROOVE FACE SEAL CONCEPTS; COMPARISON TO CONVENTIONAL FACE CONTACT SEALS IN SEALING LIQUID SODIUM (400° to 1000° F)

by Thomas N. Strom, Lawrence P. Ludwig, Gordon P. Allen,
and Robert L. Johnson

Lewis Research Center
National Aeronautics and Space Administration
Cleveland, Ohio

E-3653

SUMMARY

Conventional face contact seal performance was improved by incorporation of the spiral-groove geometry. Both conventional face contact seals and seals with spiral grooves were used to seal liquid sodium at a pressure of 20 pounds per square inch gage (14.0 N/cm^2 gage), and a sliding velocity of 79 feet per second (24 m/sec). In comparison with conventional face contact seals, seals with spiral grooves had negligible leakage. The wear and contact patterns indicated that the spiral-groove seal operated with separation of the sealing surfaces, which is necessary for long life. Supporting studies (sealing oil) on face contact seals employing the spiral-geometry is discussed.

Successful low-leakage operation was not achieved with conventional face contact seals having carbide seal seats and nosepieces (hard on hard). Thermal and pressure distortions caused edge contact, wear, and scoring. Conventional face contact seals having seal seats and nosepieces with wear-in properties (soft on hard) showed more leakage than those with carbide sealing surfaces.

INTRODUCTION

Shaft seals for containment of alkali liquid metals have applications in space power conversion systems (ref. 1). The design of these seals pre-

sents formidable problems because of high liquid temperatures (to 1337° F (725° C) for low-power systems)(ref. 2), lightweight requirement, and extremely low leakage-rate allowance of the order of several pounds per year. In addition, a high degree of reliability must be maintained for periods of 1 to 3 years of essentially unattended operation. Additional application areas for alkali metal shaft seals are found in pumps for liquid-metal flight control systems (ref. 3) and in homopolar electric machines utilizing liquid metals to transfer high-density currents (ref. 4).

The face contact seal has not been successfully applied in long-term operation as the primary seal in direct contact with alkali liquid metals. However, it is potentially a compact and complete seal system and therefore is worthy of investigation.

For long life (1 to 3 yr) and high reliability, the seal must operate with separation between the sliding surfaces (seal dam). Sliding contact of solid surfaces would probably be permissible at startup and shutdown. Separation of sliding surfaces of an argon gas seal has been accomplished by employing wavy sealing surfaces which produce a hydrodynamic life (ref. 5). In addition to surface waviness, other possible features responsible for, or contributing to, hydrodynamic separation are (1) cavitation caused by minute surface discontinuities and roughness (ref. 6), (2) axial vibration, or squeeze-film effect (ref. 7), (3) nutating motion of the seal nosepiece (ref. 7), and (4) thermal wedge effect (ref. 8).

It is herein suggested that by incorporating the viscoseal principle (in the form of a spiral groove) into the face seal, sealing surface separation and low-leakage rates can be obtained simultaneously. (Reference 9 presents a theoretical analysis of the viscoseal principles.) The sealing-

surface separation at operating speeds will ensure long seal life, and the pumping effect of the spiral-groove geometry will provide low leakage rates.

The objectives of this work were to investigate (using liquid sodium as the sealed fluid) the following:

(1) Sealing and hydrodynamic effects of the spiral groove used in conjunction with the face contact seal

(2) Leakage rates of conventional face contact seals without spiral grooves

(3) Wear characteristics of various candidate seal material combinations in conventional face contact seals

Since surface damage must be avoided on seal startup and shutdown, attention was given to sliding materials suggested by the literature. (Materials are discussed in the TEST SEALS section of this report.) This investigation was conducted with a bellows face contact seal in direct contact with liquid sodium under pressure. Surface speeds to 79 feet per second (24 m/sec) and temperatures to 1000° F (538° C) were investigated. Supporting studies using oil as the sealed fluid were made with face contact seals incorporating spiral geometry. Also, preliminary studies were made on the spiral-feed groove geometry in oil. Additional details on some of the material herein can be found in the author's papers (refs. 10, 11, and 12).

APPARATUS AND PROCEDURE

Studies Sealing Sodium

Figure 1 is a schematic diagram of the seal assembly and experimental apparatus. The rotating seal seat is attached to the horizontal shaft which is supported radially and axially by externally pressurized gas bearings

After the containment vessel is filled, the leakage-rate monitoring tank is filled to the predetermined level. The argon pressure can be remotely changed to provide various pressure differentials across the seal. Sodium temperature in the containment and support vessel is maintained by a surrounding induction coil (fig. 3). Seal leakage results in a lowering of the sodium level (changing the float position) in the leakage-rate monitoring tank. The float position is monitored by a differential transformer, the output of which is continuously recorded.

The sodium system is cleaned by the "hot flushing" technique. In this hot flushing procedure, the system is filled with sodium, soaked at operating temperatures, and then the sodium is passed back to the reservoir through the sample leg bypass line. This process is repeated several times. The oxide content is determined from a sample trapped between valves A and B (fig. 3) in the sample bypass line. The oxide content, determined by the mercury amalagamation method (ref. 14), ranged between 10 and 100 parts per million.

The seal components and housing parts were degreased, scrubbed with levigated alumina, and cleaned ultrasonically in a chlorofluorocarbon before installation in the rig. This procedure produced seal components free of hydrocarbon films and polishing media. The seal seat face runout was limited to a maximum of 0.0005 inch per inch (0.0005 cm/cm) of diameter and averaged approximately 0.0003 inch per inch (0.0003 cm/cm) of diameter. By calculation, the inertia forces at operating speeds due to this runout are not sufficient by themselves to lift the seal nosepiece out of contact with the seal seat. Before sodium was introduced, the seal was checked

(not shown). The shaft is driven by a variable speed electric drive and step-up transmission; shaft speed is monitored by a magnetic pickup. The seal housing and bellows assembly is mounted in a containment and support vessel that is filled with liquid sodium and pressurized to the operating pressure. The seal nosepiece, which is piloted by three pins (figs. 1 and 2), is held against the seal seat by a hydraulic force and by a bellows spring force. Relative motion occurs between the sealing surfaces. The bellows, besides providing a mechanical spring force, also serves as a secondary seal and allows axial motion of the seal nosepiece. Roller bearing support (not shown) for the containment and support vessel permits axial movement for controlling the amount of bellows spring force. This axial movement is controlled by means of an air-operated piston mounted outside the enclosure (fig. 3). The enclosure is pressurized slightly above ambient pressure with argon to ensure an inert environment around the containment and support vessel.

The sodium-supply and leakage-rate monitoring system is shown schematically in figure 3. Before transferring sodium, the enclosure, the containment vessel, and the leakage monitoring tank are successively evacuated and purged with argon several times to remove air. In order to transfer the sodium, the leakage monitoring tank is vented, the sample bypass leg is closed, and the reservoir is pressurized. Sodium is passed through the 20- and 5-micron filters and then to the containment vessel. The reservoir temperature is held at approximately 220° F (104° C), which is high enough to ensure transfer but low enough to allow sodium oxide precipitation and filtration. Oxide solubility is 20 parts per million at 220° F (104° C)(ref. 13).

for proper assembly by pressurizing with argon and measuring the leakage.

Supporting Studies Sealing Oil

Figure 4 is a cross section of the seal assembly and experimental apparatus. An optical flat (non-rotating) was used as a seal seat to permit observation of the interface. The carrier was fixed to the shaft and served to pilot the nosepiece. A series of 8 helical springs provided mechanical force tending to close the sealing gap. A rubber "O" ring secondary seal provide a leak tight seal and permitted axial movement of the nosepiece. Oil, which used as the test fluid, was introduced thru a tap in the base. (Only the case with oil pressure at the nosepiece ID was studied experimentally.) A capacitance probe mounted to the seal seat provided a measurement of film thickness in the sealing gap and the optical flat permitted high speed photographic study of the interface.

TEST SEALS

Fundamentals

The principle of seal pressure balance is reviewed herein since a pressure balanced seal is usually necessary for long life, high-speed applications. The thrust force due to pressurizing the bellows can be completely or partly balanced out; as a result, none or only a small fraction of the bellows thrust force acts on the sealing surfaces. The principle of pressure balancing is illustrated in figure 5 for an internally pressurized seal in which the bellows has been replaced by a piston ring ("O" ring) and spring for purposes of illustration. If the piston ring is placed on the nosepiece outside diameter (fig. 5(a)), the sealed pressure force (rectangular

area) exceeds the gap pressure force (triangular area) and the nosepiece is forced against the seal; this is a pressure-loaded seal. If the piston ring is placed on the nosepiece inside diameter, the sealed pressure force no longer acts on the nosepiece and the gap pressure force opens the seal (fig. 5(b)). However, a diameter can be selected for the piston ring such that the sealed pressure force nearly balances the gap pressure force (fig. 5(c)); this is a pressure-balanced seal. The degree of pressure balance selected depends on the degree to which the gap pressure profile can be predicted and controlled. A complete description of the seal balance must consider the following:

(1) Closing force changes due to shift of the bellows mean effective diameter with pressure

(2) Pressure profile changes under the seal dam due to distortion, surface waviness, and nonparallel sealing surfaces (dam)

(3) Spring force of the bellows

(4) Development of pressures under the seal dam due to hydrodynamic effects and fluid phase change effects

(5) Inertia forces due to seal seat runout

The preceding factors vary widely among different applications, and selection of seal balance is largely dependent on experience.

The success of a conventional face contact seal depends largely on what occurs at the seal gap (sliding surfaces). The leakage rate varies with the cube of the gap height (fig. 5(c)), and lubrication and dynamics within the gap determine power loss and wear life. The following are various possible modes of operation:

(1) Continuous or near-continuous rubbing contact between solid surfaces (This mode of operation is suitable for finite life or low-speed applications.)

(2) Separation of the sliding surfaces (except, perhaps, at startup or shutdown)(This mode of operation is necessary for long life and high-speed applications.)

(3) Operation under conditions intermediate between (1) and (2)

To meet the high seal reliability and low-power-loss requirements of the space power system, the seals must operate with separation of the sliding seal surfaces. Basically, this interface separation can be achieved by hydrostatic forces, by hydrodynamic forces, or by combined hydrostatic and hydrodynamic forces. Hydrostatic seals would have too much leakage for the space power applications and are beyond the scope of this report. Therefore, the objective is to produce separation of the sealing surfaces by hydrodynamic forces.

In general, theories and explanations for separation of sealing surfaces are based on the hydrodynamic lifting effects of minute surface discontinuities, cavitation, surface waviness, axial vibration, thermal wedges, and nutation of the seal nosepiece. These microscopic geometric and interface dynamics are difficult to control and to produce consistently. Further, the separation produced by these hydrodynamic effects usually leads to leakage.

A better approach is to use a seal geometry which will produce hydrodynamic separation forces in conjunction with pumping action to inhibit leakage. The spiral groove fits these requirements. This was, therefore, the approach taken in this investigation. The spiral groove can be incorporated in the face contact seal and offers the theoretical possibility of zero leakage with sealing surface separation (zero wear).

Seal Materials for Liquid Sodium

No exact rules exist for selecting sliding material combinations for sodium or sodium-potassium environments. The obvious requirement is that of chemical compatibility with the alkali metal at the seal operating temperature.

The material selection for the rubbing faces is made more difficult by the poor boundary lubricating properties of sodium. As pointed out in reference 2, sodium will reduce surface oxides which are normally present on metals and which are beneficial in hindering adhesion of sliding surfaces in the boundary lubrication regime. In addition, the viscosity of sodium (a significant factor in both hydrodynamic and boundary lubricating regimes) at the boiling point is 2×10^{-8} reyn (2.9×10^{-6} (lb)(sec)/ft^2 or 0.14 cP) (ref. 2), which is only 1/100 of the viscosity of SAE 10 oil at room temperature.

Investigators have tested many rubbing combinations in sodium and in sodium-potassium alloys. The results of these tests show that the majority of successful rubbing combinations employ a hard alloy cermet or oxide for one or both of the rubbing surfaces (refs. 15 to 17). As an example, in an evaluation test of material wear and adhesion in sodium at temperatures to 1000° F (538° C), the harder combinations showed better resistance to adhesive wear than did the softer material combinations (ref. 16).

Good results were obtained with soft on hard combinations in reference 18, which reports substantial wear-in of copper on tungsten carbide, and of copper on tungsten, and the subsequent development of a hydrody-

namic lift component (due to wear-in) capable of supporting 10 000 pounds per square inch (6900 N/cm^2) in a sodium-potassium alloy at 482° F (250° C).

Reference 19 suggests that the formation of sodium molybdate (Na_2MoO_4) films was beneficial in reducing friction and wear of a molybdenum couple in sodium. However, a thermochemical analysis indicates that the oxides of molybdenum are chemically unstable in liquid sodium except in the presence of large concentrations of sodium oxide. Reference 20 also investigated the effects of the surface films on sliding couples in sodium and concluded that the friction behavior depends to a large extent on whether the sodium dissolves the surface oxide or reacts with the metal and surface oxide to form a protecting film. Another form of surface protection is found in solid films of calcium fluoride - barium fluoride (CaF_2-BaF_2); these solid films are reported in reference 21 to be effective lubricants in liquid sodium at temperatures to 1000° F (538° C).

RESULTS AND DISCUSSION

Carbide Seal Rings (Hard on Hard Combination)

In Conventional Face Contact Seals

Sealing Liquid Sodium

Carbide nosepieces mated to carbide seal seats were evaluated because it has been reported (refs. 15 to 17) that the majority of successful combinations for sliding contact in alkali metals employ a carbide for one or both surfaces. Table I lists the carbide materials evaluated, the pertinent parameters, and the results. In general, operation with a carbide nosepiece mated to a carbide seal seat was not successful. The leakage rates were

either initially excessive or increased with running time to high levels because of sealing surface wear.

Thermal distortion. - The wear patterns indicated that significant thermal distortion occurred in each carbide combination evaluated (table I). Distortions are induced by thermal gradients in the seal seat and nosepiece and produce contact initially at the inner diameter of the sealing surfaces, as shown exaggeratedly in figure 6. Since carbide materials are very hard (85 to 94 Rockwell A) and have high elastic moduli (56×10^6 to 91×10^6 psi, 39 to 63×10^6 N/cm^2), the wear-in and conformability properties are practically nonexistent, and thermal distortions become significant factors in contact stress and in the lifting-force pressure profile across the sealing surfaces. The magnitude of the thermal distortions is determined by the spherical shape assumed by the seal seat and nosepiece (fig. 6) when a temperature gradient exists. When end constraints are neglected, reference 22 gives the radius of the curvature of this sphere as

$$\frac{1}{r} = \frac{\alpha\,\Delta t}{h} \tag{1}$$

where r is the radius of the curvature of the sphere, α the thermal expansion coefficient, Δt the axial temperature gradient, and h the axial ring thickness. Since the thermal gradient $\Delta t/h$ is inversely proportional to the thermal conductivity β,

$$\frac{1}{r} \approx \frac{\alpha}{\beta} \tag{2}$$

Therefore, the magnitude of thermal distortion increases as the ratio of

thermal expansion coefficient over the thermal conductivity increases. Table II lists this ratio for several candidate seal materials; the larger values indicate greater distortion.

These comparative values suggest that the carbides and molybdenum are candidate seal materials. For example, molybdenum should have 1/20 of the distortion of 347 stainless steel. However, despite the favorable α/β, the carbide and molybdenum seal rings indicated excessive distortion as evidenced by edge contact.

An example of excessive distortion is given in figure 7 which shows the condition of a titanium carbide nosepiece after a short period (40 min) of operation in sodium at a temperature of 740° F (393° C) and a sliding velocity of 79 feet per second (24 m/sec). Except for the portion near the inner edge, the majority of the surface shows no evidence of rubbing contact. Under the condition of thermal distortion, the inner edge would be expected to contact first. However, the inner and outer edges have a slight dropoff because of the lapping operation. This dropoff also occurred in the nosepiece; thus, contact occurs first at a diameter slightly larger than the inside diameter. Figure 8 shows the wear pattern on a tungsten carbide seal seat which was typical of hard on hard combinations. At various points around the seal seat a surface profile trace was taken across the sealing surfaces, and a photomicrograph of the corresponding area was matched to the surface profile trace. Distortions caused initial contact near the inside diameter of the sealing dam on the nosepiece. The wear, heaviest near the inside diameter of the wear track, decreased to near zero at the outside diameter of the wear track.

In general, effective lubrication of the carbide seal seats and nosepiece

was not obtained. In addition to wear (figs. 7 and 8), the surfaces showed evidence of heat checking (fig. 9), which is indicative of excessive sliding surface temperatures.

Leakage. - Leakage rates of the carbide combinations (table I) were not predictable; in general, they were initially high and increased to excessive levels after short running periods. One run, with a titanium carbide nosepiece mated to a tungsten carbide seal seat, did not show an increase in leakage rate, and this was attributed to development of a hydrodynamic lubricating film between the sealing surfaces. Inspection revealed that the surfaces were in good condition but had nonuniform contact (fig. 10) because of surface waviness. This slight surface waviness could have developed a hydrodynamic film which would account for the constant leakage rate of 0.61 cubic inch per hour (10 cm^3/hr) and the good surface condition. A leakage rate of 0.61 cubic inch per hour (10 cm^3/hr) is excessive for the space power system application, but for applications in which this rate is tolerable, the beneficial effect of surface waviness should not be overlooked.

Figure 11 shows the leakage trends which were evident throughout the evaluation. The leakage increased with speed because of the combined effect of centrifugal force and larger average gap produced by seal runout. The increase in leakage with pressure is expected, but the minimums exhibited at certain pressures are unexplained.

Conventional Face Contact Seals Sealing Sodium With One Sliding Surface Having a Conformability Property (Soft on Hard Combination)

Thermal distortion proved to be a major problem with seals having car-

bide seal seats sliding against carbide nosepiece rings (hard on hard combinations); therefore, various seal ring materials having a wear-in or conformability property were evaluated. Table III includes the seal ring materials evaluated, pertinent parameters, and results.

Foam metal rings impregnated with calcium fluoride - barium fluoride. - Nickel-base alloy and nickel foam metal impregnated with calcium fluoride - barium fluoride showed the desired conformability to thermal distortion. Sliding contact over the full width of the sealing surface was obtained by the wear-in process as shown in figure 12. The tungsten carbide mating nosepiece surface showed no indication of scoring, metal transfer, or adhesive wear. Thus the calcium fluoride - barium fluoride impregnated material was performing the lubricating function as pointed out in reference 21. However, the leakage rates were excessive (table III) for the space power type of application.

Copper nosepieces and molybdenum seal seats. - In a further effort to attain a wear-in or conformability property, copper and molybdenum nosepieces were run against tungsten carbide and against each other. (Reference 18 reported a wear-in property with copper mated to tungsten carbide, and reference 19 reported formation of beneficial surface films on molybdenum in sodium.) The copper and tungsten carbide combination showed no evidence of scoring or metal transfer. However, the sodium leakage rate was excessive (table III), and the wear-in process did not reduce seal leakage. The molybdenum and tungsten carbide combination showed scoring and adhesive wear of the molybdenum surface (fig. 13), and the leakage was excessive. A combination of copper sliding against molybdenum showed extreme surface distress and operated only for 3 minutes.

Face Seal With Spiral Grooves Sealing Sodium

Face seals were constructed with spiral grooves on the high pressure side of the sealing surfaces (dam). One assembly incorporated grooves on the nosepiece (fig. 14); grooves on the seal seat were also evaluated (fig. 15). The motion of the rotating seal seat causes the spiral grooves to produce an inward pumping action against leakage of sodium.

Leakage and wear. - Table IV lists the leakage results and operating conditions. A copper nosepiece (fig. 14), with spiral grooves and a seal seat of tungsten carbide operated in liquid sodium for 4 hours at 20 pounds per square inch gage (14 N/cm^2 gage) with leakage less than the estimated detection limit of 0.02 cubic inch per hour (0.30 cm^3/hr). Inspection of the sealing surfaces revealed several local wear areas on the copper nosepiece; the major portion of the surface showed no evidence of rubbing contact.

Another assembly evaluated consisted of a plain copper nosepiece and a molybdenum spiral-groove seal seat. This combination was operated for 9 hours at various speeds and at a sodium pressure of 20 pounds per square inch gage (14 N/cm^2 gage) with negligible leakage. Visual observation of the seal below 64 feet per second (20 m/sec) indicated leakage of intermittent minute drops of liquid sodium which oxidized into small pepper-size flakes. (Visual observation required the opening of the enclosure; thus some oxygen was present around the seal area during the inspection.) Above 64 feet per second (20 m/sec) these drops could not be observed. The sealing surfaces were in excellent condition after the 9 hours of operation (fig. 15) and showed that rubbing contact had occurred over most of the surface (prob-

ably at startup). As mentioned previously, the combination of copper and molybdenum operated only 3 minutes in the conventional face seal configuration and showed extreme surface distress even though the temperature, pressure, and speed were lower. It was concluded that the spiral-groove seal operated with interface separation. This conclusion is based on the excellent surface condition of the copper and molybdenum surfaces and on the fact that this poor wear combination (copper on molybdenum) was operated successfully at a relatively high temperature of 500° F (260° C) and a speed of 64 feet per second (20 m/sec) for 9 hours in a poor boundary lubricant, sodium. Before startup, the seal showed no leakage; this indicated good contact and flatness at the sealing surfaces. At shutdown, the seal showed slight leakage at zero rotation which indicated that some change in surface flatness had occurred. Spiral grooves were also incorporated into carbide seal seats and were mated to carbide nosepieces (in four tests). The results were similar to those in table IV and in each of the four tests sliding surfaces were in excellent condition after several hours of operation (figs. 16 and 17) in liquid sodium.

Spiral seal operating mode. - On startup the pumping action of the spiral grooves displaces the sodium inward from the seal dam; thus the seal tends to become pressure loaded (fig. 5(a)). This pressure load must be offset by hydrodynamic forces to prevent excessive rubbing contact. It is postulated that hydrodynamic forces arise from a slider bearing effect of the spiral-groove land area and from the pressure patterns developed by the spiral grooves. (Reference 10 includes a discussion of viscoseal pressure patterns.) The two arrangements evaluated in this study concerned pressurized liquid at the inside diameter of the seal interface;

(fig. 18) one arrangement had spiral grooves on the nonrotating nosepiece, and the other had spiral grooves on the rotating seal seat. Arrangements which were not evaluated involved pressurized liquid at the outside diameter of the seal interface (fig. 19). In this latter case, centrifugal force works to prevent leakage, and low-leakage rates should be more readily attainable than in the arrangement with pressurized liquid at the inside diameter.

SUPPORTING SPIRAL SEAL STUDIES IN OIL

Operation of the spiral groove geometry was visually observed using an optical flat as the seal seat and using oil as the sealed fluid. A sketch of the arrangement is shown in figure 4. The spiral groove pattern was etched into the rotating member, which, in this case, was a brass nosepiece (fig. 20).

At zero speed the nosepiece is in contact with the seal seat and the seal functions as a conventional face contact seal. When rotation starts the nosepiece is lifted out of contact with the seal seat and a film of lubricant is established over the land area. When rotation stops the nosepiece again seats against the seal seat. The lift and torque is shown in figure 21 which is a plot of film thickness (as measured with capacitance probes) and torque against seal rpm. Figure 22 shows the spiral groove seal in operation with oil as the sealed fluid. A strobe light was used to stop the action and the liquid-gas interface is clearly defined in the groove area. The presence of an oil film over the land area is proof of positive separation of the sealing surfaces. It was observed that increasing speeds above ~1400 rpm resulted in instability of the liquid and gas interface in the form of sheets of liquid

leaving the interface due to centrifugal force. This centrifugal effect did not lead to excessive leakage since the spiral grooves pumped most of this interface loss back into the wetted portion of the seal. Increased lift and increased torque were measured above this speed (1400 rpm) as shown in figure 21. For the design with the sealed liquid at the sealing dam O.D. centrifugal force will work to prevent leakage. However, it must be noted that this oil leakage may be necessary to support an appreciable amount of pressure load, since the load carrying capacity of this seal design is governed by the amount of oil in the groove available to give the hydrodynamic lift effect. It was found that at speeds of 1600 rpm, increasing the sealed fluid pressure from 0 to 60 pounds per square inch gage (0-42 N/cm^2 gage) had very little effect on the seal lift.

SPIRAL-FEED GROOVE SEAL STUDIES IN OIL

Preliminary studies were made sealing oil using the spiral feed groove seal design. Figure 4 shows the general arrangement of the experimental facility and figure 23 is an overall view of the seal nosepiece with the etched spiral feed groove pattern. The seal was designed for and operated with the sealed liquid (oil) at the I.D., however, the spiral feed groove pattern can be applied to the case in which the sealed liquid is at the O.D. At static conditions the seal functions as a face contact seal and the sealed pressure is effective to the sealing dam I.D. The pressure balance (spring force plus pressure force) is selected to provide a force that tends to close the seal. Oil is fed to the spiral groove via holes drilled in the seal face and a 0.010 inch (0.025 cm) deep circumferential feed groove. When rotation starts a liquid to gas interface is formed within the outer portion of the spiral pattern when operating within the designed pressure range. The

pressure at the feed groove is approximately the same as the pressure at the I.D. of the inner land. The inner spiral increases the pressure from the sealed pressure to a maximum at the junction of the inner spiral and inside diameter dam. The outer spiral "pumps" against the supply pressure.

The pumping effort of the inner spiral pattern produces an "opening" force to balance the seal "closing" force, and the height of the sealing gap is a function of the closing force and the pressure generation capacity of the spiral patterns. Figure 24 shows film thickness and torque as a function of speed when operating in oil. It should be noted that the film thickness is greater for the spiral-feed groove seal than that of the spiral groove seal. With the spiral groove seal, the lift (film thickness) is due to hydrodynamic forces over the land area, however, with the spiral-feed groove the life is due to hydrodynamic forces generated within the groove and across the inner dam (see refs. 9 and 12 for viscoseal theory).

Spiral-Herringbone Concept

Another concept of balancing the pressure loading forces (i.e., increasing the lift forces) could be accomplished using the spiral herringbone pattern shown in figure 28. When rotation starts a liquid to gas interface will be formed in the outer spiral pattern when operating within the designed pressure range. The spiral increases the pressure from the sealed pressure to a maximum at the junction of the two spiral patterns. The outer spirals pump against the pressure developed by the inner spiral pattern. Thus, the outer spiral pattern must have more radial length to offset both the sealed pressure and the pumping effort of the inner spiral pattern.

Comparison of spiral-groove face seals and helical viscoseal. - The spiral-groove and spiral-feed groove seal operates with the same sealing principle as the helical viscoseal (fig. 27). However, the spiral seals are inherently more compact and in addition provides positive sealing at zero rotation. (The helical viscoseal requires an additional positive contact seal to prevent leakage at startup, shutdown, or in a static condition.) The pressure generating capacity of the helical viscoseal or spiral seal is given by reference 23 as

$$\frac{\Delta P}{L} = \frac{6U\mu(\lambda G)}{c^2} \tag{3}$$

where ΔP is the pressure differential across the seal, L the wetted seal length, U the peripheral speed, μ the agsolute viscosity, λ the sealing coefficient, G the geometry factor, and c the clearance. It is pointed out that the pressure gradient is a function of c^2. In a spiral face seals, a much smaller clearance c is more readily attained than with the cylindrical viscoseal. For example, a 0.005-inch (0.013-cm) radial clearance is required in some viscoseal designs because of shaft runout and vibration. But a spiral face seals can operate with less than 0.0010-inch (0.0025-cm) clearance. Hence, the spiral-groove face seal is inherently smaller for the same application.

SUMMARY OF RESULTS

Conventional face contact seals and face contact seals incorporating the spiral-groove geometry were evaluated for leakage and wear when sealing liquid sodium. The following were the significant results:

1. In comparison with conventional face contact seals, the spiral groove seals showed negligible leakage and wear. Separation of the sealing surfaces due to hydrodynamic forces over the land area is postulated.

2. Static leakage of the spiral-groove face seal was similar to that of a face contact seal.

3. As compared to the helical-groove seal, the spiral-groove face seal has the following advantages:

(a) It is more compact in size because of higher pressure capacity produced by the inherently smaller seal gap.

(b) It functions as a face contact seal at startup and for shutdown.

4. Successful low-leakage operation was not achieved with conventional face contact seals (no spiral grooves) having carbide seal rings (hard on hard combination). Thermal distortions coupled with the lack of conformability (high hardness and modulus) and the poor lubricating ability of the sodium caused wear and scoring of the sealing surfaces.

5. Successful low-leakage operation was not achieved with conventional face contact seals (no spiral grooves) having soft on hard material combinations which were used in an attempt to obtain some conformability to offset thermal distortions. Generally, the sealing dam surfaces showed better contact and less scoring than did the hard on hard combinations, but leakage was not lower.

6. The feasibility of the spiral feed groove seal was demonstrated in oil sealing studies. As compared to the spiral groove seal, the spiral feed groove seal developed greater film thickness under the same operating conditions.

REFERENCES

1. A. E. King, "Screw Type Shaft Seals for Potassium Lubricated Generators," IEEE Transactions on Aerospace, vol. AS-3, June, 1965, supplement, pp. 471-479.

2. E. E. Bisson and W. J. Anderson, "Advanced Bearing Technology," NASA Special Publication 38, 1964.

3. J. R. Granan and R. C. Dumpitsch, "Pumps for Liquid-Metal Flight Controls," ASME Paper No. 66-FE-20, April, 1966.

4. G. Fournet and R. Bonnefille, "New Electrical Machines," International Science and Technology, no. 51, March 1966, pp. 38-47.

5. R. W. Kelly, G. M. Wood, and D. V. Manfredi, "Cermet Face Seals for Inert Gas Environements," ASLE Preprint No. 65 AM 4C4, May, 1965.

6. D. B. Hamilton, J. A. Walowit, and C. M. Allen, "A Theory of Lubrication by Microirregularities," Journal of Basic Engineering, vol. 88, no. 1, March 1966, pp. 177-185.

7. B. S. Nau, "Hydrodynamics of Face Seal Films," Proceedings of the Second International Conference on Fluid Sealing, Cranfield, England, April 6-8, 1964, B. S. Nau, H. S. Stephens, and D. E. Turnbull, editors, British Hydromechanics Research Association, 1964, pp. F5-61 to F5-80.

8. O. Pinkus and B. Sternlicht, Theory of Hydrodynamic Lubrication, McGraw-Hill Book Company, Inc., New York, N.Y., 1961.

9. J. Zuk, L. P. Ludwig, and R. L. Johnson, "Flow and Pressure Field Analysis of Parallel Groove Geometry For an Incompressible Fluid With Convective Inertia Effects," NASA Technical Note D-3635, September, 1966.

10. L. P. Ludwig, T. N. Strom, and G. P. Allen, "Experimental Study of End Effect and Pressure Patterns in Helical Groove Fluid Film Seal (Viscoseal)", NASA Technical Note D-3096, 1967.

11. L. P. Ludwig, T. N. Strom, G. P. Allen, and R. L. Johnson, "Improving Performance of Face Contact Seal in Liquid Sodium (400° to 1000° F) by Incorporation of Spiral-Groove Geometry", NASA Technical Note D-3942, May, 1967.

12. J. Zuk, T. N. Strom, L. P. Ludwig, and R. L. Johnson, "Convective Inertia and Gas Ingestion Effects on Flow Regimes of the Viscoseal-Theory and Experiment", presented at the ASLE Annual Meeting, Toronto, Ontario, Canada, May 1-4, 1967.

13. C. B. Jackson, editor, Liquid Metals Handbook. Sodium - NaK Supplement, AEC and Bureau of Ships Report No. TID-5277, July 1, 1955.

14. D. E. Kuivinen, "Determination of Oxygen in Liquid Alkali Metals by the Mercury Amalgamation Method," presented at the Nineteenth Meeting, Chemical Rocket Propulsion Group, St. Paul, Minn., July-August 1963.

15. D. F. Elliott, E. Holland, and K. A. Tomblin, "Some Preliminary Tests on Atomic Energy Research Establishment, Report No. AERE-R/R-1891, April 23, 1956.

16. R. B. Jerman, R. C. Williams, and D. O. Leeser, "Evaluation of Material Wear and Self-Welding in Sodium-Cooled Reactor Systems", Journal of Basic Engineering, vol. 81, no. 2, June, 1959, pp. 213-225.

17. T. Lyman, editor, Properties and Selection of Metals. Vol. 1 of Metals Handbook, American society for Metals, Metals Park, Ohio, 8th ed., 1961.

18. L. F. Coffin, Jr., "Boundary Lubrication, Wear-In and Hydrodynamic Behavior of Bearings for Liquid Metals and Other Fluids," ASLE Transactions vol. 1, no. 1, April 1958, pp. 139-150.

19. J. W. Kissel, W. A. Glaeser, and C. M. Allen, "Sliding Contact Frictional Behavior in Sodium Environments", ASLE Transactions, vol. 5, no. 1, April, 1962, pp. 39-44.

20. N. C. Balchin, "The Friction of Clean Metals Immersed in Liquid Sodium," British Journal of Applied Physics, vol. 13, November, 1962, pp. 564-569.

21. H. E. Sliney, T. N. Strom, and G. P. Allen, "Fused Fluoride Coatings as Solid Lubricants in Liquid Sodium, Hydrogen, Vacuum, and Air," NASA Technical Note D-2348, August, 1964.

22. S. Timoshenko, Strength of Materials. Part II, D. Van Nostrand Company, Inc., Princeton, N. J., 3rd ed., 1956.

23. L. P. Ludwig, T. N. Strom, and G. P. Allen, "Gas Ingestion and Sealing Capacity fo Helical Groove Fluid Film Seal (Viscoseal) Using Sodium and Water as Sealed Fluids," NASA Technical Note D-3348, March, 1966.

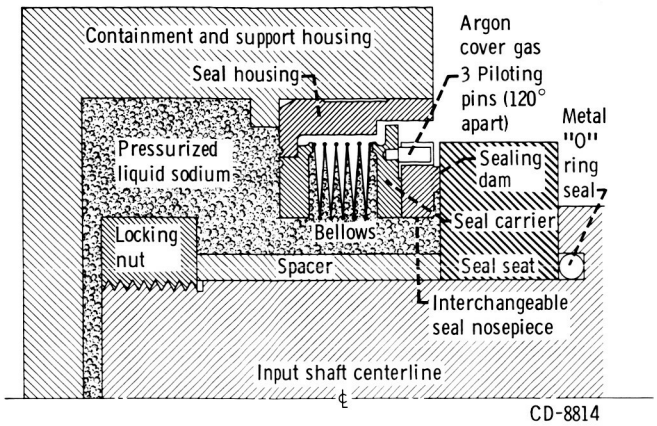

Figure 1. - Schematic diagram of face contact seal assembly and experimental apparatus.

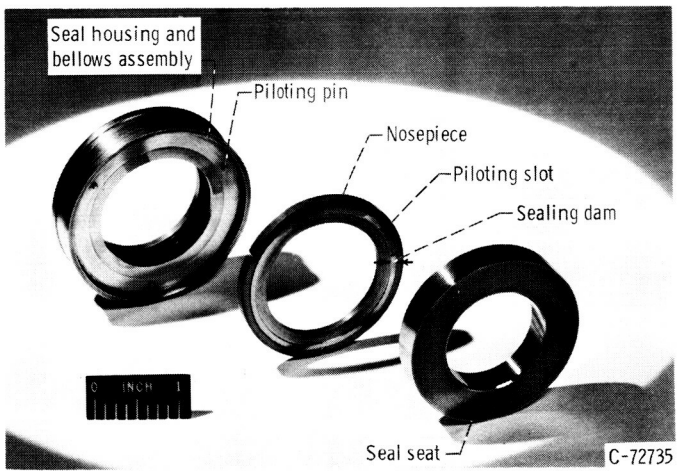

Figure 2. - Face contact seal.

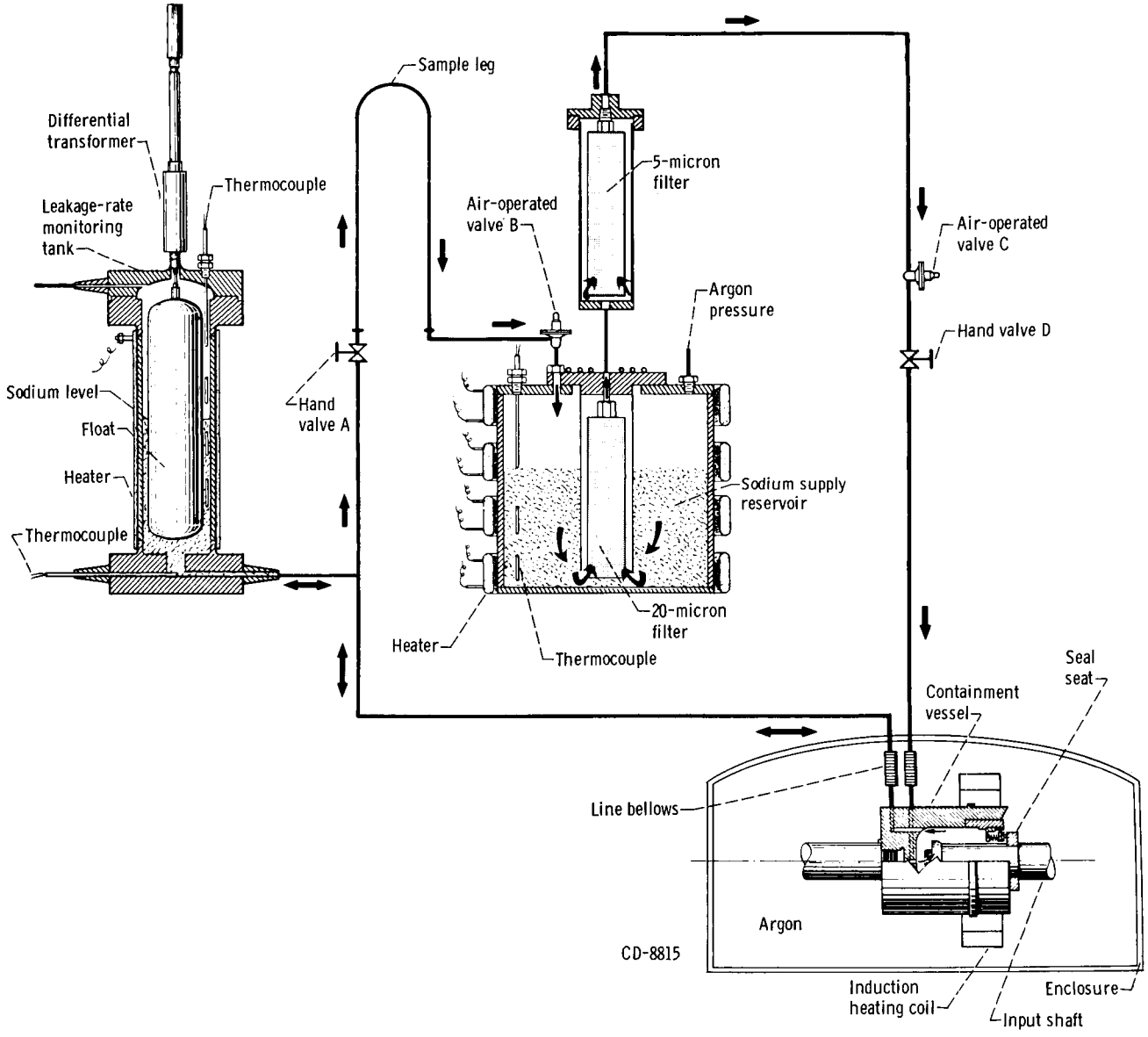

Figure 3. - Sodium supply system.

E-3653

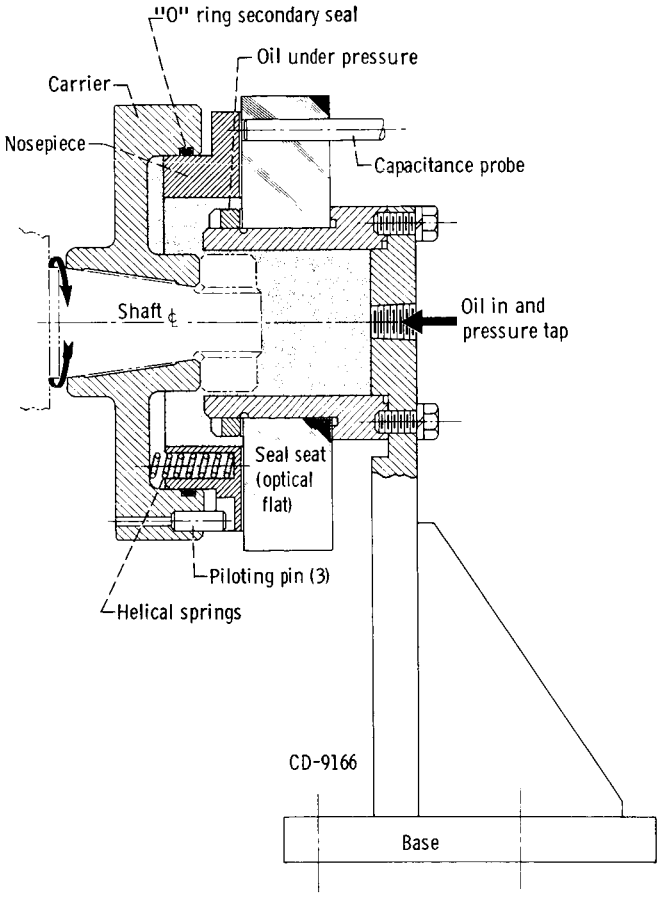

Figure 4. - Cross sectional drawing of seal assembly for supporting studies in oil.

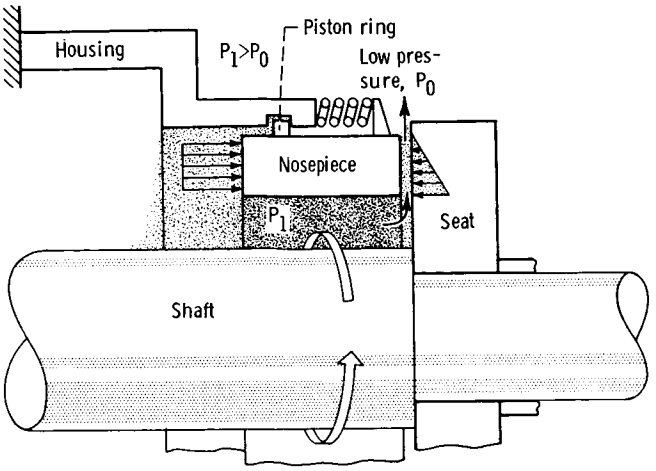

(a) Pressure loaded.

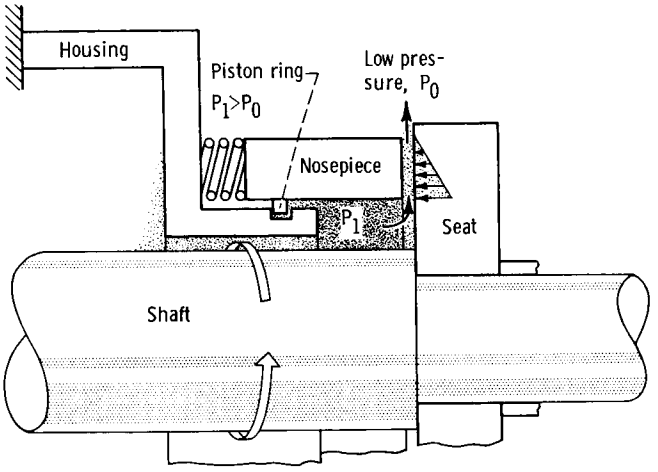

(b) Pressure unloaded.

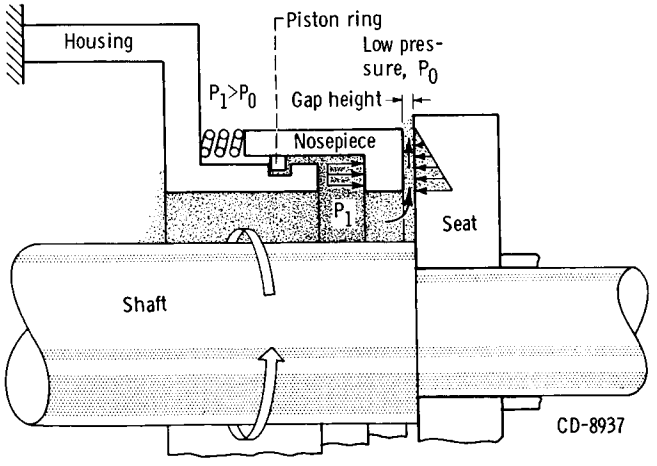

(c) Pressure balanced.

Figure 5. - Face contact seal pressure balance.

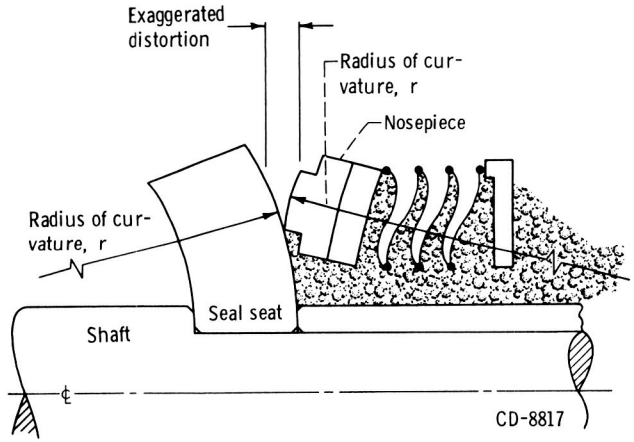

Figure 6. - Schematic diagram showing edge contact caused by axial thermal gradients.

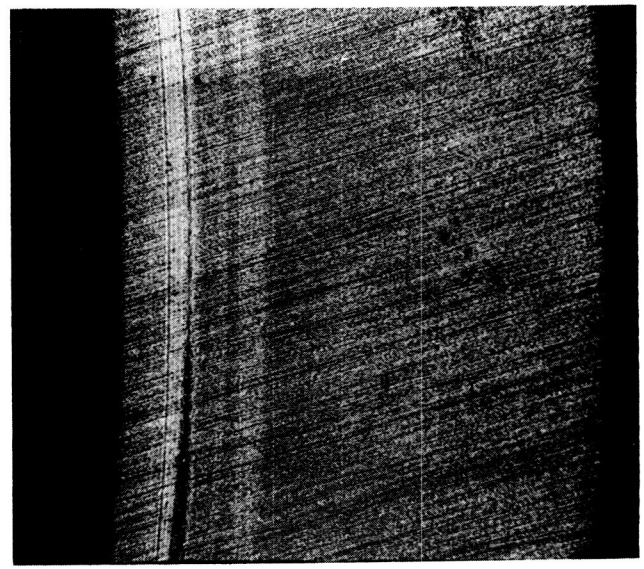

(a) Photomicrograph of surface.

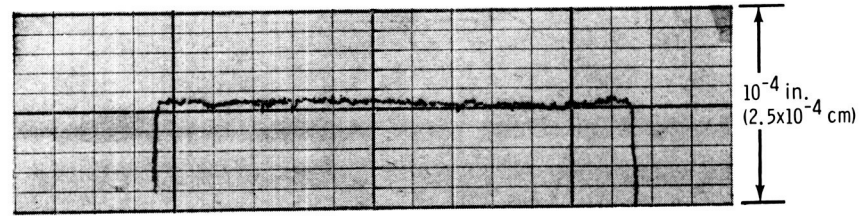

(b) Surface profile.

Figure 7. - Photomicrograph and surface profile of titanium carbide nosepiece after operation against tungsten carbide seal seat showing limited contact width. Sodium temperature, 740° F (393° C); operating time, 40 minutes; sliding velocity, 79 feet per second (24 m/sec); pressure, 30 pounds per square inch gage (20.6 N/cm^2 gage).

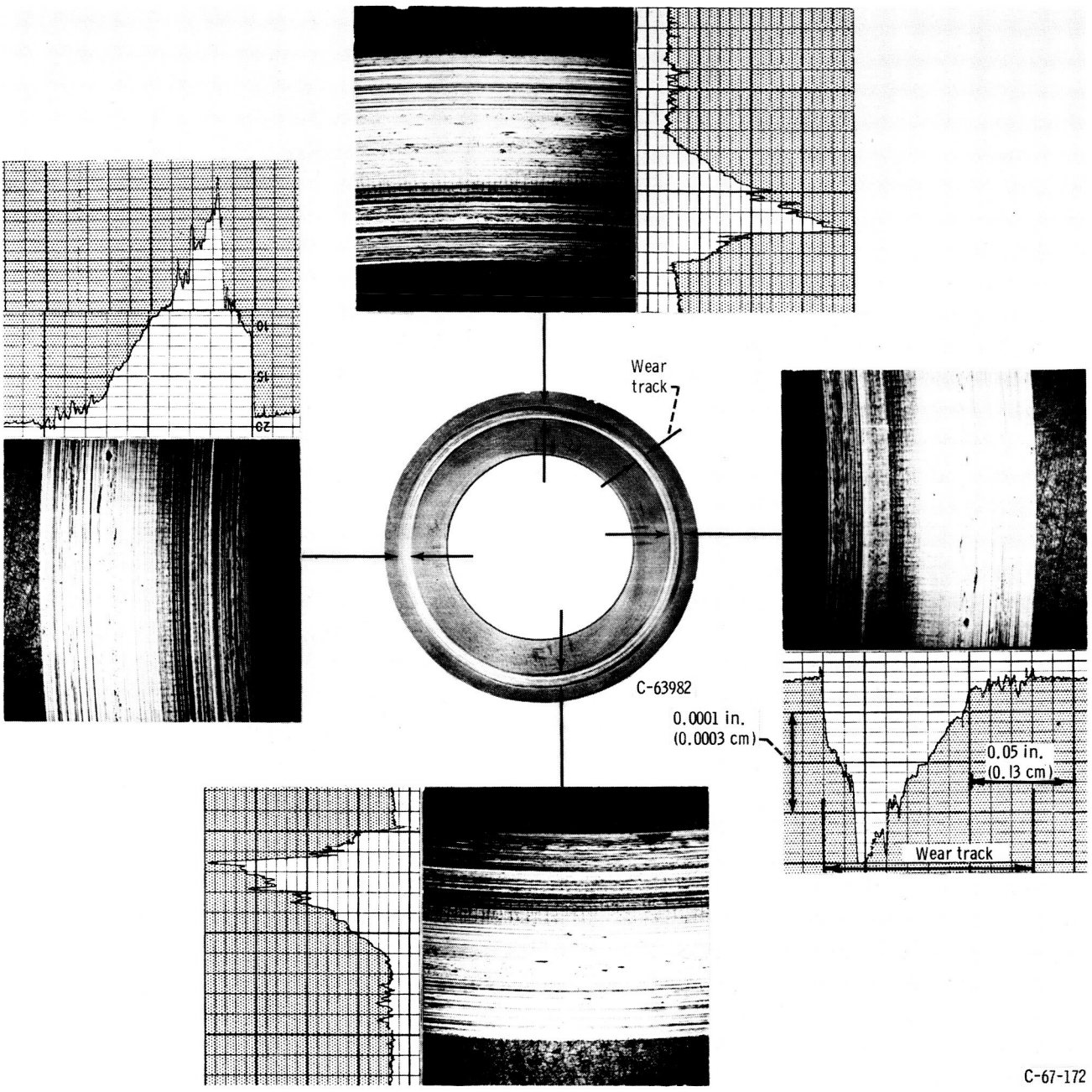

Figure 8. - Overall wear pattern, surface profile traces, and photomicrographs of tungsten carbide seal seat. Sodium temperature, 1000° F (538° C); operating time, 4 hours; sliding velocity, 79 feet per second (24 m/sec); pressure, 50 pounds per square inch gage (34 N/cm^2 gage).

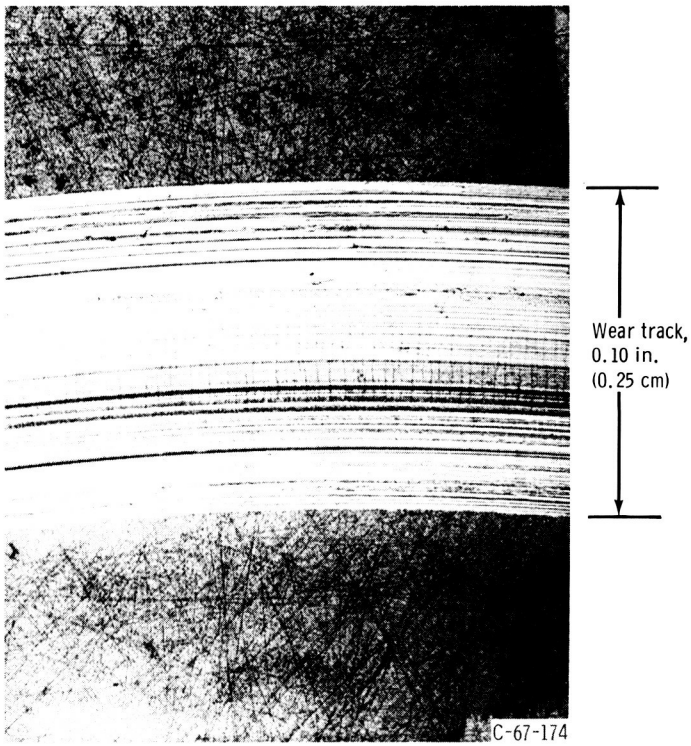

Figure 9. - Photomicrograph of tungsten carbide seal seat showing heavy scoring and heat checking. Sealed fluid, sodium; sodium temperature, 1000° F (538° C); sliding velocity, 79 feet per second (24 m/sec); sealed pressure, 50 pounds per square inch gage (34 N/cm^2 gage); mating material, titanium carbide - niobium carbide - tantalum carbide composite.

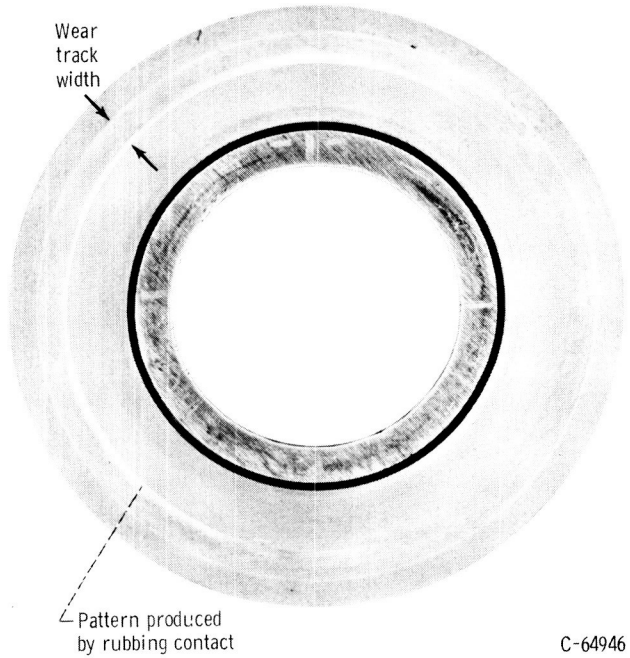

Figure 10. - Tungsten carbide seal seat showing wear pattern resulting from surface waviness. Sodium temperature, 1000° F (538° C); sliding velocity, 79 feet per second (24 m/sec); pressure, 50 pounds per square inch gage (34 N/cm^2 gage).

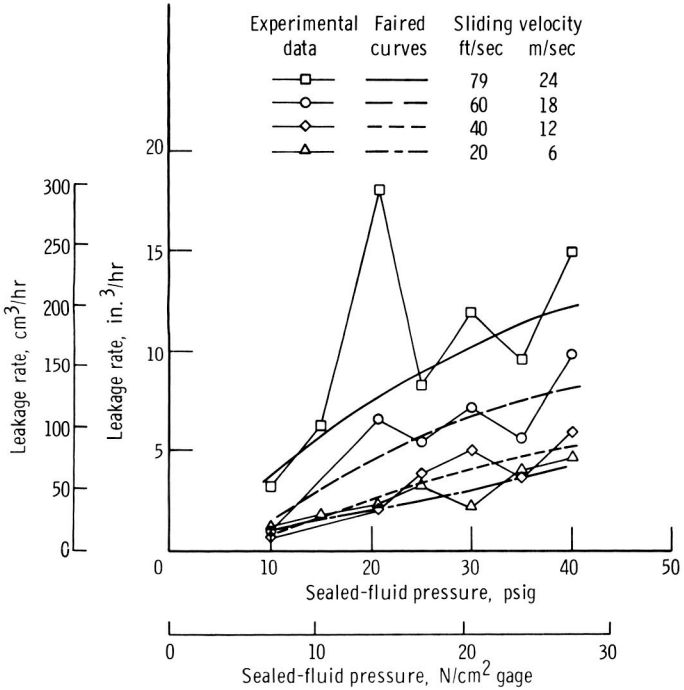

Figure 11. - Effect of speed and pressure on face-contact-seal leakage trends. Temperature, 600° F (316° C); tungsten-carbide seal seats and nosepieces; sealed fluid, sodium.

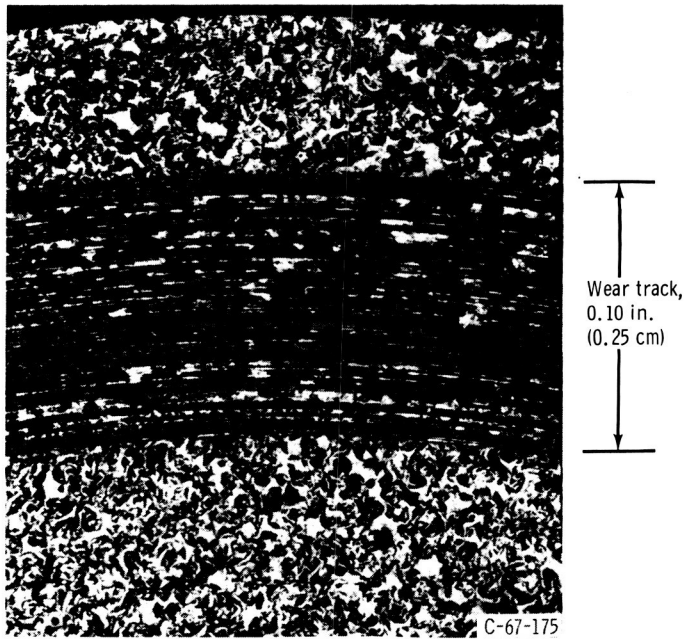

Figure 12. - Wear track on seal seat of 40-weight-percent foam nickel impregnated with calcium fluoride - barium fluoride. Sealed fluid, sodium; sodium temperature, 1000° F (538° C); sliding velocity, 79 feet per second (24 m/sec); sealed pressure, 9.5 pounds per square inch gage (6.6 N/cm^2 gage).

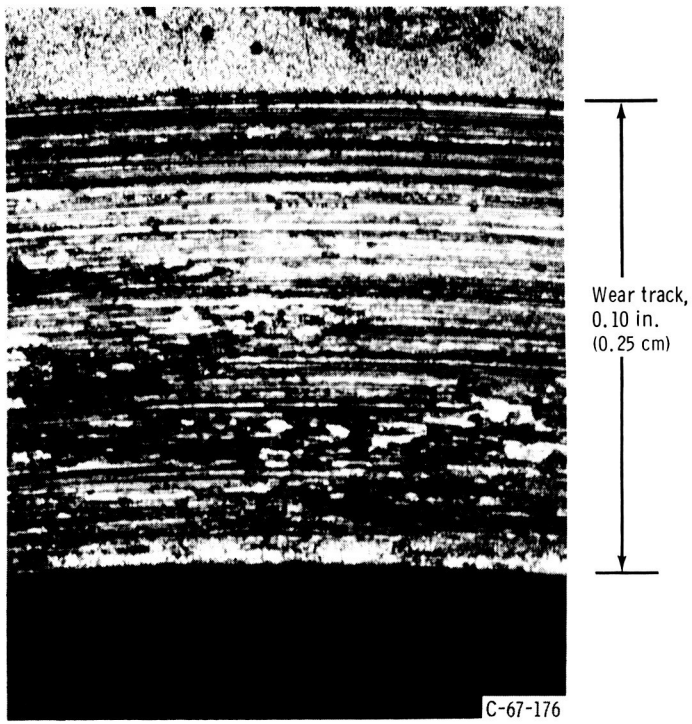

Figure 13. - Wear track on molybdenum seal seat. Sealed fluid, sodium; sodium temperature, 1000° F (538° C); sliding velocity, 79 feet per second (24 m/sec); sealed pressure, 65 pounds per square inch gage (45 N/cm^2 gage).

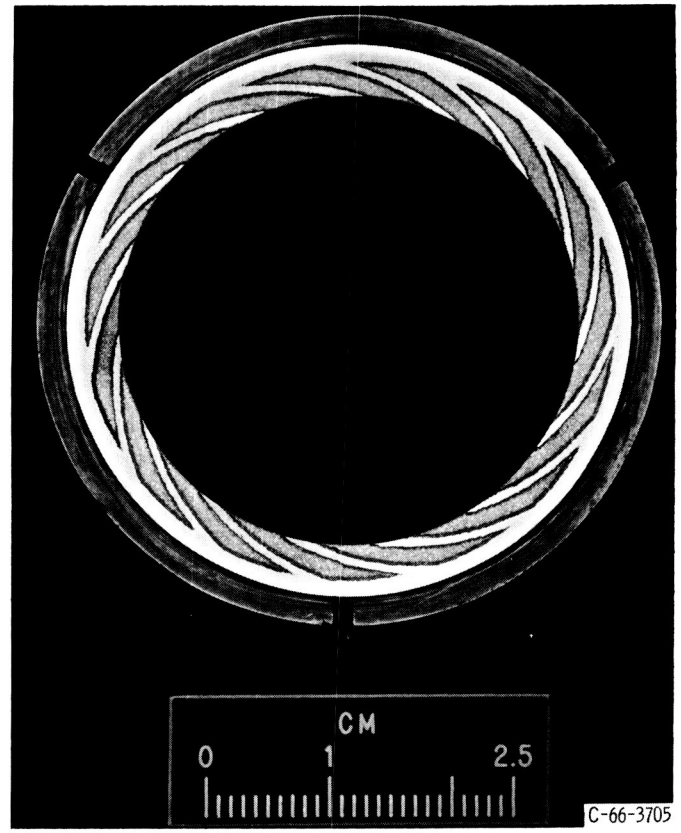

Figure 14. - Spiral-groove geometry chemically etched into copper nosepiece.

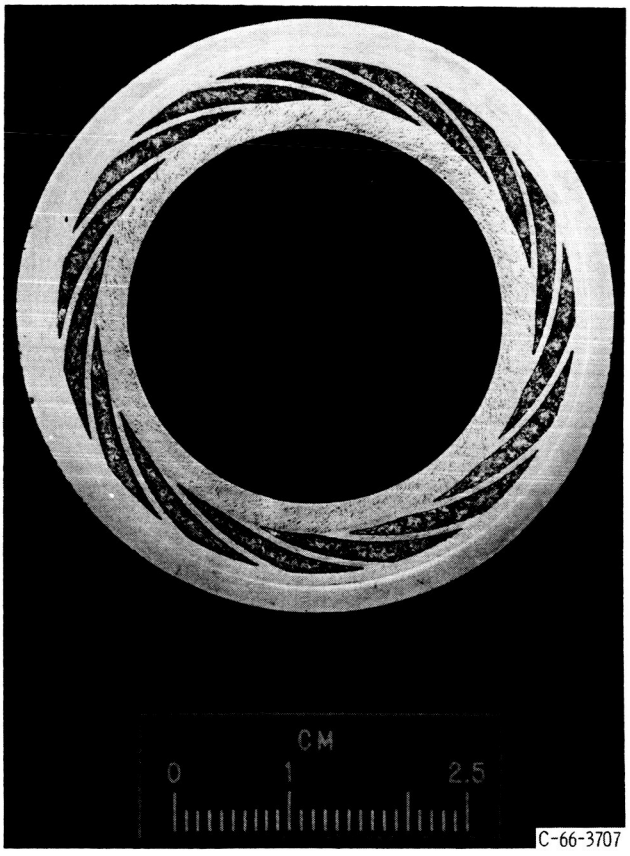

Figure 15. - Seal seat with inward-pumping spiral groove design. Material, molybdenum; groove depth .0015 inches (.0038 cm); sealed fluid, sodium; sodium temperature 500°f (260°C); operating time, 4 hours; sliding velocity, 64 feet per second (20m/sec); sealed pressure, 20 pounds per square inch, gage ($14N/cm^2$).

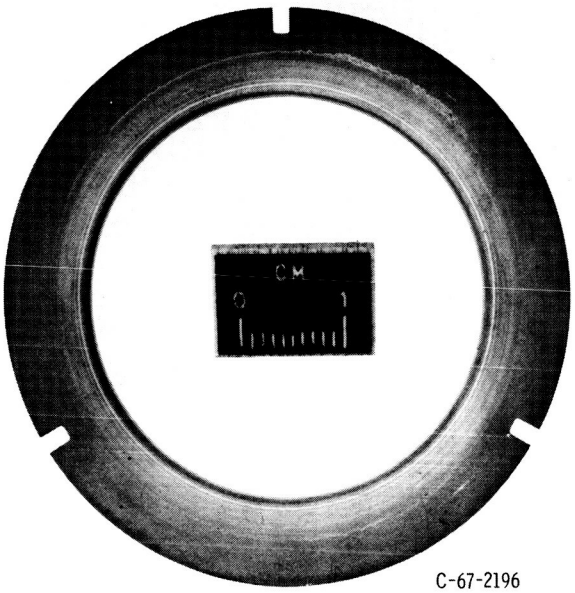

C-67-2196

(a) Seal nosepice.

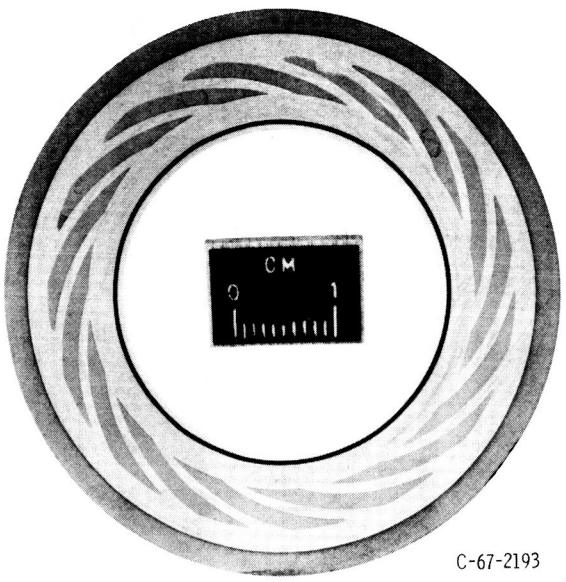

C-67-2193

(b) Seal seat.

Figure 16. - Seal nosepiece and seal seat with inward pumping spiral-groove design. Material - tungsten carbide; groove depth, .0005 inch (.0127 cm); sealed fluid, sodium; sodium temperature, 600° F (516°C); operating time 4 hours; sliding velocity, 64 feet per second (20 m/sec); sealed pressure, 20 pounds per square inch gage (14N/cm^2 gage).

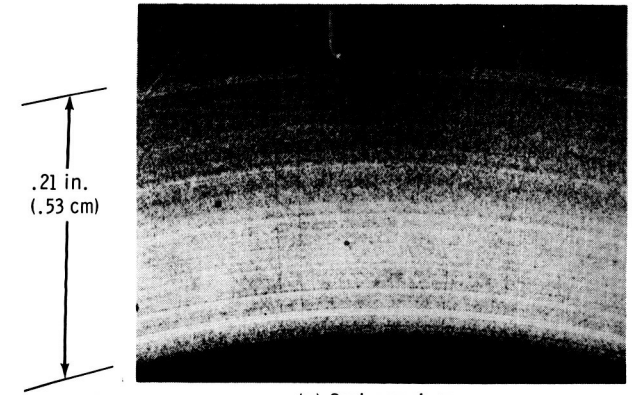

(a) Seal nosepiece.

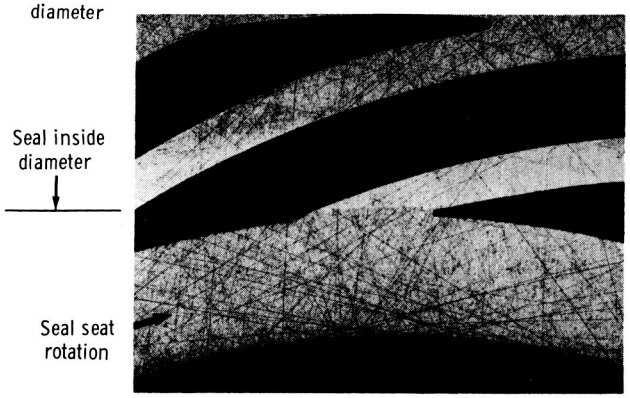

(b) Seal seat.

Figure 17. - Seal nosepiece and seal seat with inwards pumping spiral-groove design. Material - tungsten carbide; groove depth, .0005 inch (.0127 cm); sealed fluid, sodium; sodium temperature, 600° F (516° C); operating time 4 hours; sliding velocity, 64 feet per second (20 m/sec); sealed pressure, 20 pounds per square inch gage (14N/cm^2 gage).

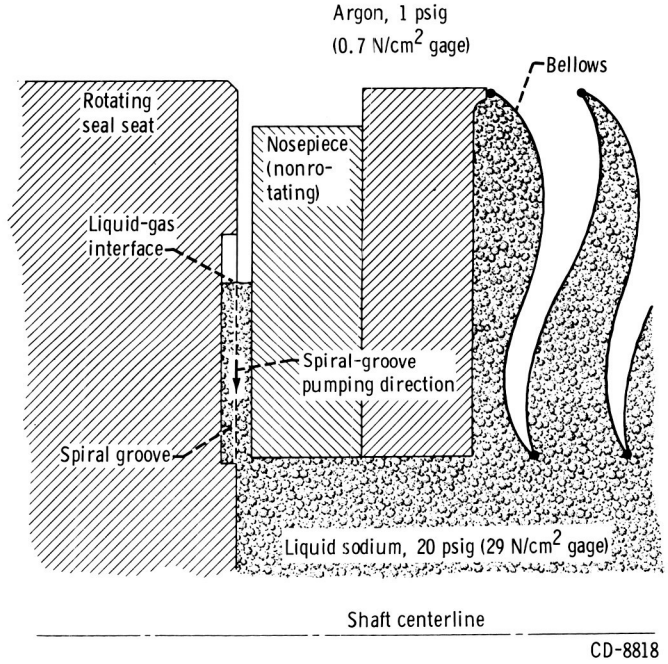

Figure 18. - Spiral-groove seal seat in operating mode.

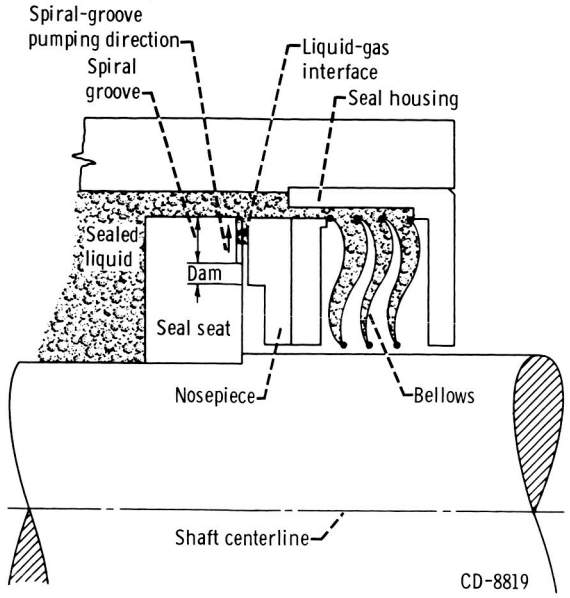

Figure 19. - Spiral-groove placement in seal seat for sealing liquid at outside diameter of seal dam.

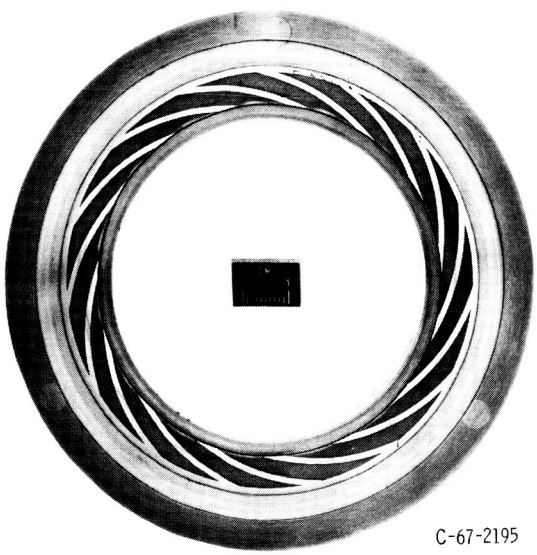

Figure 20. - Seal nose piece with chemically etched inward-pumping spiral grooves.

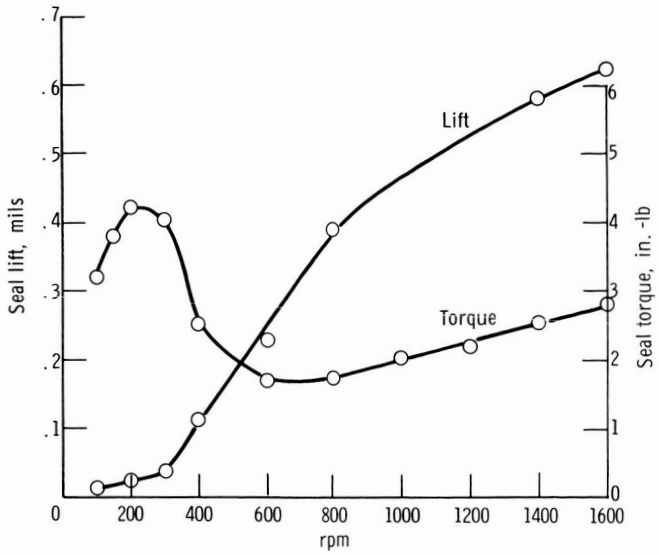

Figure 21. - Seal lift and torque at various speeds for the spiral groove seal. Sealed fluid, J-43 hydraulic oil at 20 psig. Oil temperature 100°±5° F.

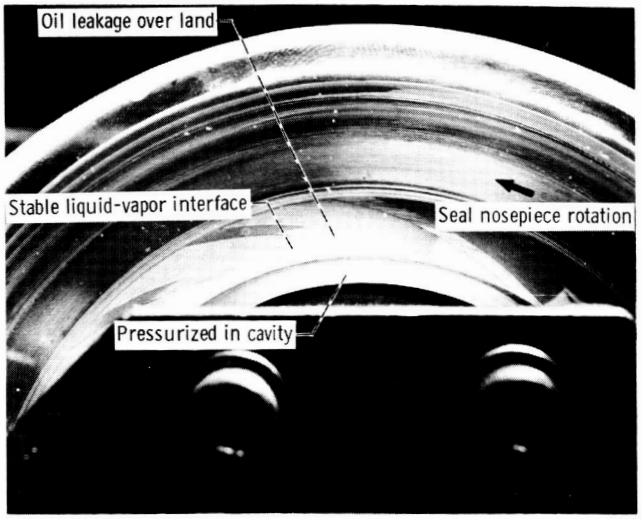

Figure 22. - Spiral groove seal as viewed through the optical flat mating surface. Speed-500 rpm, sealed fluid-J-43 hydraulic oil. Pressure 10 psi.

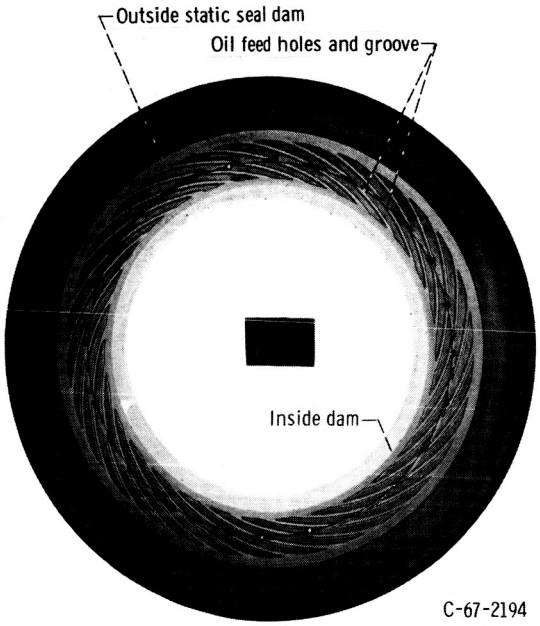

Figure 23. - Spiral-feed groove seal geometry chemically etched into brass nosepiece.

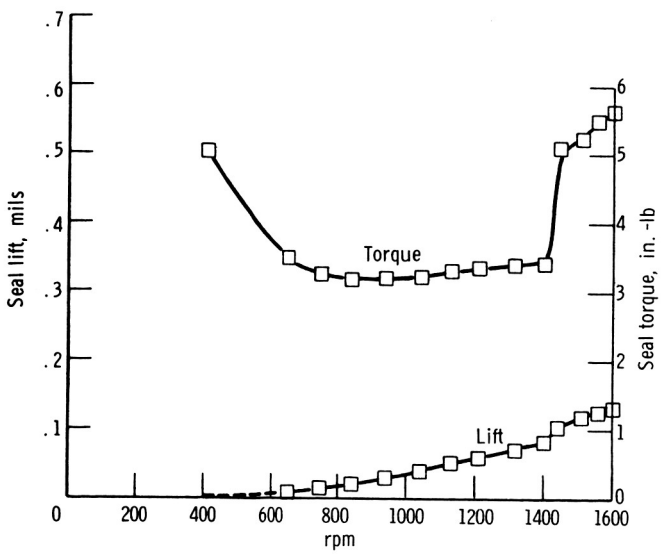

Figure 24. - Seal lift and torque at various speeds for the spiral feed groove seal. Sealed fluid, J-43 hydraulic oil at 20 psig. Oil temperature 100° ±5° F.

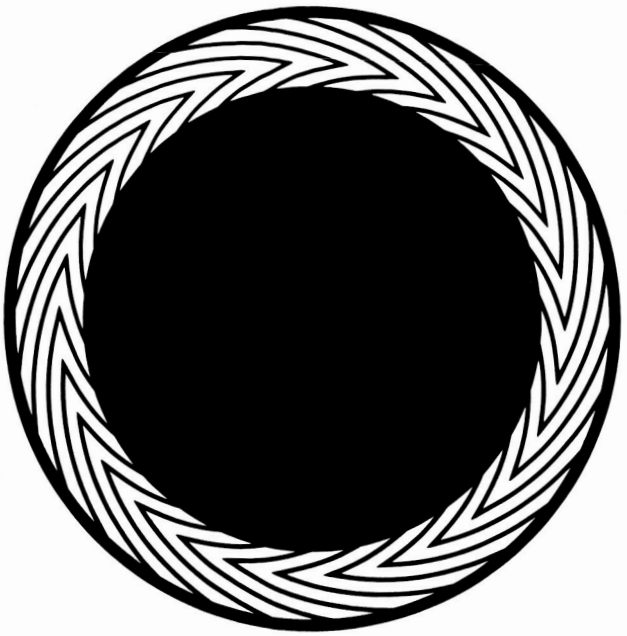

Figure 25. - Spiral-herringbone concept pattern.